Journal of the
Nigerian Mathematical Society

Vol. 39, Issue 3, pp. 353-388, 2020

LOCAL NONSIMILARITY SOLUTIONS FOR MIXED CONVECTIVE FLOW OVER A STRETCHING SHEET IN THE PRESENCE OF CHEMICAL REACTION AND HALL CURRENT

M. O. LAWAL[1] AND S. O. AJADI

ABSTRACT. This paper presents the combined effects of buoyancy forces, pressure gradient, heat source, thermal radiation, chemical reaction and Hall current on the heat and mass transfer of Newtonian fluid over a stretching sheet subjected to a nonlinear stretching velocity. The governing nonlinear partial differential equations were reduced to a system of coupled nonlinear ordinary differential equations by using an established local non-similarity transformation. The resulting equations are then solved numerically using the Midpoint Method with Richardson Extrapolation Enhancement scheme and implemented on the MAPLE 18 platform. The result reveals that axial and transverse velocity profiles increase as Hall current parameter increases; though the increase is more pronounced for the transverse velocity. The magnetic field strength was observed to reduce concentration, axial and transverse velocity profiles but increases the temperature profiles. It was also observed that increasing the nonlinear velocity parameter led to increases in the axial and transverse velocity profiles whereas it reduces the temperature and concentration profiles. In line with the physics of the problem, an increase in chemical reaction parameter reduces the concentration and the influence of Hall current parameter on both axial and transverse velocities are of great significance. The study concluded that the combined effects of thermophysical parameters such as chemical reaction, Hall current, thermal radiation and others are very significant in MHD boundary layer flow.

Keywords and phrases: Chemical reaction, Hall current, Local nonsimilarity, Stretching sheet.
2010 Mathematical Subject Classification: 35G61, 76D05 76N10, 78M25, 76W05

Received by the editors July 18, 2020; Revised: October 22, 2020; Accepted: November 17, 2020

www.nigerianmathematicalsociety.org; Journal available online at https://ojs.ictp.it/jnms/

[1]Corresponding author

1. INTRODUCTION

The problems of heat and mass transfer in the boundary layers on continuous stretching surfaces starting from the pioneering articles of Sakiadis [1] and [2] have attracted considerable attentions during the last few decades due to the numerous applications to several industrial manufacturing processes such as extrusion of plastic sheet, hot rolling, wire drawing, glass fibre and paper production, drawing of plastic films, metal spinning and the cooling of a metallic plate in a cooling bath. It is known that the combined effect of the kinematics of stretching and the simultaneous heating or cooling during such processes have a decisive influence on the quality of the final product [3]- [11].

The study of magnetohydrodynamics (MHD) viscous flows is important to industrial, technological and geothermal applications such as high-temperature plasma, cooling of nuclear reactors, liquid metal fluids, magnetohydrodynamic generators and accelerators. As a result, a significant amount of interest has been carried out to study the effects of electrically conducting fluids such as liquid metals, water mixed with little acid and others in the presence of a magnetic field on the flow and heat transfer aspects in various geometries [12]- [13].

Hall [14] observed that when an electrical current passes through a sample placed in a magnetic field, a potential proportional to the current and to the magnetic field is developed across the material in a direction perpendicular to both the current and to the magnetic field. The Hall effect is important when the magnetic field is high or when the collision frequency is low, causing the Hall parameter to be significant (Sutton and Sherman [15]). Alfven [16] discussed movement within a conducting fluid that is in the presence of a magnetic field will generate electrical currents. Owing to the magnetic field, these currents give mechanical forces which change the state of motion of the liquid. Also, Rossow [17] reported significance of transverse magnetic field that can be used to control the motion of electrically conducting fluids over a flat plate.

Muthucumaraswamy [18] investigated the effects of heat and mass transfer on a continuously moving isothermal vertical surface with uniform suction taking into account the homogeneous chemical reaction of first order. A theoretical solution of the problem are obtained in terms of exponential functions. It is observed that the velocity increases during the generative reaction and decreases in

the destructive reaction, while the concentration increases in the presence of the generative reaction.

Devi *et al.* [19] analyzed a steady MHD boundary layer flow due to an exponentially stretching sheet with radiation taking into account heat source/sink. By using a fourth order Runge-Kutta method along with shooting technique, they obtained a numerical solution which shows that the momentum boundary layer thickness decreases while both thermal and concentration boundary layer thicknesses increase with an increase in the magnetic field intensity and the radiation reduces the temperature. Gangadhar and Bhaskar [20] analyzed the problem of chemically reacting MHD boundary layer flow of heat and mass transfer over a moving vertical plate in a porous medium with suction. The heat source/sink effects in thermal convection are significant where there exist a high temperature differences between the surface (e.g. space craft body) and the ambient fluid.

Bhattacharyya [21] analyzed the effect of heat source/sink on MHD flow and heat transfer over a shrinking sheet with mass suction. Employing finite difference method using quasilinearization technique, it is found that velocity inside the boundary layer increases with increase in wall mass suction and magnetic field and accordingly the thickness of the momentum boundary layer decreases. The temperature decreases with Hartmann number, Prandtl number and heat sink parameter and the temperature increases with heat source parameter. Furthermore, for strong heat source, heat absorption at the sheet occurs. Reddy *et al.* [22] discussed the growing need for chemical reactions in chemical and hydrometallurgical industries which require the study of heat and mass transfer with chemical reaction. It was observed that the presence of a foreign mass in water or air causes some kind of chemical reaction.

Makinde *et al.* [23] carried out numerical study of chemically reacting hydromagnetic fluid with Soret-Dufour effects and a convective surface boundary condition using Nachtsheim-Swigert Shooting iteration technique in conjuction with Runge-Kutta 6th order integration Scheme. Magnetic field has been observed to retard the flow in the boundary layer but simultaneously enhance temperatures and concentration values. The growth of both momentum and thermal boundary layer thicknesses are enhanced by mass diffusion effect while the concentration field is appreciably influenced by the thermal diffusion.

Shateyi *et al*. [24] studied the Hall effect on MHD flow and heat transfer over an unsteady stretching permeable surface in the presence of thermal radiation and heat source/sink. A computational iterative approach known as Spectral Local Linearization Method (SLLM) blended with Chebyshev Spectral Method is employed and when compared with Matlab bvp4c routine technique, an excellent agreement is observed. The velocity components are enhanced as the Hall parameter increases, the fluid temperature increases with increasing values of thermal radiation as well as a heat source.

Rao *et al*. [25] considered unsteady MHD free convective heat and mass transfer flow past a semi-infinite vertical permeable moving plate with heat absorption, radiation, chemical reaction and Soret effects using perturbation techniques. The fluid velocity is found to increase with increasing thermal Grashof number and mass Grashof number. The increase in heat source and radiation effects caused the reduction in the fluid temperature which resulted in decrease in the fluid velocity, while increase in Soret effect caused the reduction in the concentration distribution and this resulted in decreasing in the fluid velocity.

Fatunmbi *et al*. [26] examined mixed convective and heat transfer analysis of hydromagnetic Micropolar fluid past a heated inclined sheet which stretches nonlinearly along the direction of flow.

This study was motivated by the works of some renown authors, particularly Bhattacharyya [21], Shateyi and Gerald [24], Makinde *et al*. [23] and Fatunmbi *et al*. [26]. Basically, this work contributes to the body of knowledge by employing local nonsimilarity transformation approach for a nonsimilar boundary layer flow problem. However, the knowledge of the flow geometry and mechanism shows that some of the thermophysical parameters like Hall current effect, chemical reaction, thermal radiation, buoyancy forces, heat source/sink, pressure gradient and nonlinear velocity that were not considered on the heat and mass transfer on MHD fluid in some of the previous works cannot be totally neglected and have not been articulated together in a single study.

The governing equations modelling MHD flow, heat and mass transfer over stretching surfaces are highly nonlinear therefore making exact solutions impossible to obtain. Therefore, numerical solutions have always been developed and modified, with a bid to get more accurate and stable solutions. This study presents the effects of combining some prominent thermophysical parameters on an unsteady chemically reactive MHD mixed convective heat and mass

transfer flow over a stretching sheet in presence of Hall current using the local non-similarity method implemented on the MAPLE 18 platform.

1.2 Research Questions

Based on the aforementioned, the following research questions are appropriate:

(i) How does the use of MMRE compare with SLLM?
(ii) What are the contributions of Chemical reaction and Hall current on the axial and transverse velocities?
(iii) How does increasing suction affect the axial and transverse velocities?
(iv) And what are the effects of other embedded parameters on the variables of state(velocity, temperature and concentration)?

2. FORMULATION OF THE PROBLEM

We consider a two-dimensional, unsteady mixed convective MHD chemically reactive flow of an electrically conducting, viscous fluid radiating over a continuously moving stretching sheet with a chemical reaction source based on the one-step exothermic reaction. The boundary layer is assumed flat while the reaction source is placed in the viscous region as shown in Fig. 1. The governing equations of the MHD boundary layer flow in the presence of uniform transverse magnetic field in the viscous region are:

$$\begin{aligned}\frac{\partial u}{\partial t}+u\frac{\partial u}{\partial x}+v\frac{\partial u}{\partial y} =&\nu\frac{\partial^2 u}{\partial y^2}-\frac{1}{\rho}\frac{\partial P}{\partial x}-\frac{\sigma B^2}{\rho(1+m^2)}(u+mw)\\ &+g\beta_c(C-C_\infty)+g\beta_T(T-T_\infty),\end{aligned} \tag{1}$$

$$\frac{\partial w}{\partial t}+u\frac{\partial w}{\partial x}+v\frac{\partial w}{\partial y}=\nu\frac{\partial^2 w}{\partial y^2}+\frac{\sigma B^2}{\rho(1+m^2)}(mu-w), \tag{2}$$

$$\frac{\partial T}{\partial t}+u\frac{\partial T}{\partial x}+v\frac{\partial T}{\partial y}=\frac{\kappa}{\rho C_p}\frac{\partial^2 T}{\partial y^2}+\frac{Q_o}{\rho C_p}(T-T_\infty)-\frac{1}{\rho C_p}\frac{\partial q_r}{\partial y}, \tag{3}$$

and

$$\frac{\partial C}{\partial t}+u\frac{\partial C}{\partial x}+v\frac{\partial C}{\partial y}=D\frac{\partial^2 C}{\partial y^2}-K_r(C-C_\infty)e^{-\frac{E}{RT}}. \tag{4}$$

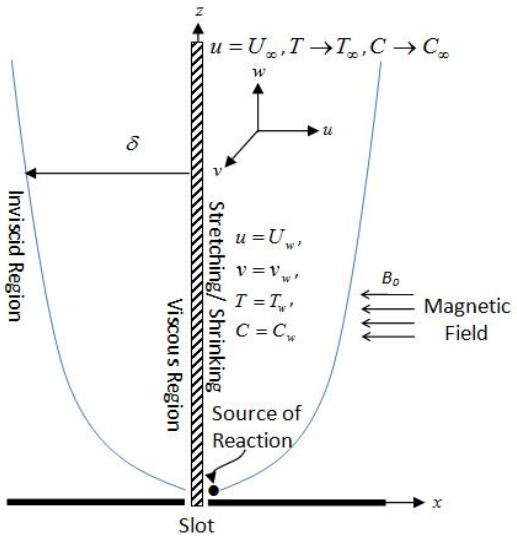

Fig. 1. Schematic diagram of the flow.

The associated initial and boundary conditions for the present problem are

$$t = 0: \ u = 0, \ v = 0, \ T = T_w, \ C = C_w \text{ at } y = 0, \tag{5}$$

$$t > 0: \ u = U_w(x,t), \ v = v_w, \ T = T_w(x,t), \ C = C_w \text{ at } y = 0, \tag{6}$$

$$t > 0: \ u \to U_\infty(x,t), \ w \to 0, \ T \to T_\infty, \ C \to C_\infty, \text{ as } y \to \infty. \tag{7}$$

Following Ishak *et al.*[27] and Khan *et al.*[28] for the similarity transformation, we introduce the following dimensionless quantities and parameters as functions of f, g, θ, ϕ, a pseudosimilarity variable η and non-similarity variable ξ:

$$\begin{aligned}
&\psi = \sqrt{\frac{\lambda\nu b}{1-ct}} x^{\frac{j+1}{2}} f(\xi,\eta), \ \eta = \sqrt{\frac{\lambda b}{\nu(1-ct)}} y x^{\frac{j-1}{2}}, \\
&\xi = v_w \sqrt{\frac{1-ct}{\lambda\nu b}} x^{\frac{1-j}{2}}, \ w = \frac{\lambda b}{1-ct} x^j g(\xi,\eta), \ U_w = \frac{\lambda b x^j}{1-ct}, \\
&\theta(\xi,\eta) = \frac{T - T_\infty}{T_w - T_\infty}, \ \phi(\xi,\eta) = \frac{C - C_\infty}{C_w - C_\infty}, \ U_\infty = \frac{\lambda a x^j}{1-ct}.
\end{aligned} \tag{8}$$

The sheet surface temperature and concentration which varies with the distance x from the origin (slot) and time t are:

$$T_w = T_\infty + T_0 \frac{\lambda^2 b x^{2j}}{2\nu(1-ct)^{3/2}}, \ C_w = C_\infty + C_0 \frac{\lambda^2 b x^{2j}}{2\nu(1-ct)^{3/2}}, \tag{9}$$

where λ is a scaling parameter of the dimension L^{1-j} and $L \neq 0$. The expressions $U_w(x,t)$, $U_\infty(x,t)$, $T_w(x,t)$, $C_w(x,t)$ are valid only

for the time $t < \frac{1}{c}$ (i.e. $ct < 1$) and $c > 0$ (positive constant). T_0 is the reference temperature such that $0 \leq T_0 \leq T_w$.
By using the Rosseland diffusion approximation, the radiation heat flux is given by

$$q_r = -\frac{4\sigma^*}{3K^*}\frac{\partial T^4}{\partial y}, \tag{10}$$

where σ^* and K^* are the Stefan-Boltzman constant and the Rosseland mean absorption coefficient respectively. We assume that the temperature differences within the flow are sufficiently small such that T^4 may by expressed as a linear function of temperature. Expanding T^4 in a Taylor series about T_∞ and neglecting higher order terms we obtain $T^4 \approx 4T_\infty^3 T - 3T_\infty^4$ substituting this in (10) and finally into the fourth term on right hand side of (3) we obtain

$$\frac{\partial q_r}{\partial y} = -\frac{16\sigma^* T_\infty^3}{3K^*}\frac{\partial^2 T}{\partial y^2}. \tag{11}$$

Local Nonsimilarity Approach
Problems involving mixed convection, surface mass transfer, effect of suction or injection of fluid at the wall, variation in wall temperature, variation in free-stream velocity, inclination angle effects in boundary layers analysis are usually not self similar or locally similar or admissible to similarity solution because of the embedded parameters that are usually marked with the presence of dimensional variables. According to Minkowycz and Sparrow [29], the first step in the development of the solution method is to transform the problem from the x, y coordinate system to the ξ, η system. The coordinate η, which involves both x and y, with x denoting the streamwise coordinate and y the transverse coordinate, may be termed a pseudo-similarity variable; it is chosen to reduce to a true similarity variable for boundary layers which are similar. In the same vein, ξ is related to x and is so chosen that x does not appear explicitly in the transformed conservation equations or the boundary conditions, hence, the need for this solution approach.

By applying this nonsimilarity variables and quantities above in (8) and (9), the continuity equation (1) is automatically satisfied and the governing partial differential equations are transformed into

a system of coupled non-linear ODE as shown below:

$$f''' + \frac{j+1}{2} ff'' + j[\omega^2 - (f')^2] - A_x(f' + \frac{1}{2}\eta f'' - \frac{1}{2}\xi F') + Gr_x\theta + Gc_x\phi - \frac{M}{(1+m^2)}(f' + mg) = \frac{1-j}{2}\xi\left[f'\frac{\partial f'}{\partial \xi} - f''\frac{\partial f}{\partial \xi}\right], \tag{12}$$

$$g'' + [\frac{j+1}{2} fg' - jf'g] - A_x(g + \frac{1}{2}\eta g' - \frac{1}{2}\xi G) + \frac{M}{(1+m^2)}(mf' - g) = \frac{1-j}{2}\xi\left[f'\frac{\partial g}{\partial \xi} - g'\frac{\partial f}{\partial \xi}\right], \tag{13}$$

$$(1+\frac{4}{3}R)\theta'' + Pr(\frac{j+1}{2} f\theta' - 2jf'\theta) - \frac{PrA_x}{2}(3\theta + \eta\theta' - \xi X) - \delta_x\theta = Pr\frac{1-j}{2}\xi\left[f'\frac{\partial \theta}{\partial \xi} - \theta'\frac{\partial f}{\partial \xi}\right], \tag{14}$$

$$\phi'' + Sc(\frac{j+1}{2} f\phi' - 2jf'\phi) - \frac{ScA_x}{2}(3\phi + \eta\phi' - \xi Y) - ScLrRe_x\phi e^{\frac{\theta}{1+\epsilon\theta}} = Sc\frac{1-j}{2}\xi\left[f'\frac{\partial \phi}{\partial \xi} - \phi'\frac{\partial f}{\partial \xi}\right]. \tag{15}$$

The corresponding dimensionless initial and boundary conditions are

$$f'(\xi,\eta) = 1,\ g(\xi,\eta) = 0,\ \theta(\xi,\eta) = 1,\ \phi(\xi,\eta) = 1,\ \text{at } \eta = 0,\quad f' \to \omega,\ g \to 0,\ \theta \to 0,\ \phi \to 0 \text{ as } \eta \to \infty. \tag{16}$$

Where primes denote the differentiation with respect to η and

$A_x = \frac{c}{\lambda b x^{j-1}}$, $Gr_x = \frac{g\beta_T(T_w - T_\infty)x}{U_w^2}$, $Gc_x = \frac{g\beta_c(C_w - C_\infty)x}{U_w^2}$,
$R = \frac{4\sigma^* T_\infty^3}{\kappa K^*}$, $m = \omega_e\tau_e$, $M = \frac{\sigma B_0^2}{\rho U_w}x$, $\omega = \frac{a}{b}$, $\delta_x = \frac{\nu Q_o}{\kappa U_w}x$,
$Pr = \frac{\mu C_p}{\kappa}$, $Sc = \frac{\nu}{D}$, $\epsilon = \frac{-E}{R^* T_\infty}$, $Re_x = \frac{xU_w}{\nu}$, $Lr = \frac{\nu K_r}{U_w^2} e^{\frac{-E}{R^* T_\infty}}$.

$V_w = -(\frac{\nu U_w}{\xi})^{\frac{1}{2}} f(\xi, 0)$ represents the mass transfer at the surface with $f(\xi, 0) = f_w$ where $f_w < 0$ and $f_w > 0$ represent injection and suction respectively. $A_x = \frac{M_x}{1+m^2}$ for satisfactory bounbary condition.

The local similarity solution often regarded as the first level of truncation is computationally attractive but leads to numerical results of uncertain accuracy. This coincides with when the respective right hand side (RHS) terms of equations (12) - (15);

$\xi\left[f'\dfrac{\partial f'}{\partial\xi}-f''\dfrac{\partial f}{\partial\xi}\right]$, $\xi\left[f'\dfrac{\partial g}{\partial\xi}-g'\dfrac{\partial f}{\partial\xi}\right]$, $\xi\left[f'\dfrac{\partial\theta}{\partial\xi}-\theta'\dfrac{\partial f}{\partial\xi}\right]$ and $\xi\left[f'\dfrac{\partial\phi}{\partial\xi}-\phi'\dfrac{\partial f}{\partial\xi}\right]$ are deleted or neglected. Furthermore, the errors incurred by employing the local similarity method are markedly greater, the uncertainty concerning the validity of this assumption of neglecting RHS or when ξ is sufficiently small is a weakness of the local similarity method.

However, in order to overcome the mentioned drawback in solving non-similar boundary layer equations, the local nonsimilarity solution approach presented by Sparrow *et al*. [30]; Sparrow and Yu [31] can be adopted to third level of truncation(or three-equation model). No error had been committed by stopping at the second level though higher levels of truncations can be obtained by proceeding along lines similar to the second level. It is well known that the second level truncation is a relatively good approximation since the third level truncation makes no significant contribution to the solution (Sparrow and Yu [31]).

The governing equations for f, g, θ and ϕ at the second level of truncation(local nonsimilarity) in equations (12) - (15) are retained without approximation. The auxiliary equations for F, G, X and Y are derived by taking $\dfrac{\partial}{\partial\xi}$ of (12) - (15), introducing $\dfrac{\partial f}{\partial\xi}=F$, $\dfrac{\partial g}{\partial\xi}=G$, $\dfrac{\partial\theta}{\partial\xi}=X$ and $\dfrac{\partial\phi}{\partial\xi}=Y$ and then respectively truncating the terms $\xi\left[\dfrac{\partial}{\partial\xi}\left(f'F'-f''F\right)\right]$, $\xi\left[\dfrac{\partial}{\partial\xi}\left(f'G-g'F\right)\right]$, $\xi\left[\dfrac{\partial}{\partial\xi}\left(f'X-\theta'F\right)\right]$ and $\xi\left[\dfrac{\partial}{\partial\xi}\left(f'Y-\phi'F\right)\right]$ in equations (21) - (24). According to this concept as reported by Minkowycz and Sparrow [29], Sparrow *et al*. [30] and Mohamad *et al*. [32], the RHS of the equations are assumed to be sufficiently small so that it may be approximated by zero. Boundary conditions for F, G, X and Y are also obtained by differentiating (16) with respect to ξ and deleting $\dfrac{\partial F}{\partial\xi}$, $\dfrac{\partial G}{\partial\xi}$, $\dfrac{\partial X}{\partial\xi}$ and $\dfrac{\partial Y}{\partial\xi}$.

Therefore, the complete set of the governing, auxiliary equations obtained from second level truncation model and their respective

boundary conditions are

$$f''' + \frac{j+1}{2} ff'' + j(\omega^2 - f'^2) - A_x(f' + \frac{1}{2}\eta f'' - \frac{1}{2}\xi F') + Gr_x\theta + Gc_x\phi - \frac{M}{(1+m^2)}(f' + mg) = \frac{1-j}{2}\xi\left(f'F' - f''F\right), \tag{17}$$

$$g'' + (\frac{j+1}{2} fg' - jf'g) - A_x(g + \frac{1}{2}\eta g' - \frac{1}{2}\xi G) + \frac{M}{(1+m^2)}(mf' - g) = \frac{1-j}{2}\xi\left[f'G - g'F\right], \tag{18}$$

$$\frac{1}{Pr}(1 + \frac{4}{3}R)\theta'' + (\frac{j+1}{2} f\theta' - 2jf'\theta) - \frac{A_x}{2}(3\theta + \eta\theta' - \xi X) + \delta_x\theta = \frac{1-j}{2}\xi\left[f'X - \theta'F\right], \tag{19}$$

$$\frac{1}{Sc}\phi'' + (\frac{j+1}{2} f\phi' - 2jf'\phi) - \frac{A_x}{2}(3\phi + \eta\phi' - \xi Y) - LrRe_x\phi e^{\frac{\theta}{1+\in\theta}} = \frac{1-j}{2}\xi\left[f'Y - \phi'F\right], \tag{20}$$

$$F''' + \frac{j+1}{2}\left(fF'' + f''F\right) - 2jf'F' - A_x(\frac{1}{2}F' + \frac{1}{2}\eta F'') + Gr_xX + Gc_xY - \frac{1-j}{2}(f'F' - f''F) - \frac{M}{(1+m^2)}(F' + mG) = 0, \tag{21}$$

$$G'' + \frac{j+1}{2}(fG' + g'F) - j(f'G + F'g) - A_x(\frac{1}{2}G + \frac{1}{2}\eta G') - \frac{1-j}{2}(f'G - g'F) + \frac{M}{(1+m^2)}(mF' - G) = 0, \tag{22}$$

$$\frac{1}{Pr}(1 + \frac{4}{3}R)X'' + \frac{j+1}{2}(fX' + \theta'F) - 2j(f'X + F'\theta) + \delta_xX - \frac{A_x}{2}(2X + \eta X) - \frac{1-j}{2}(f'X - \theta'F) = 0, \tag{23}$$

$$\frac{1}{Sc}Y'' + \frac{j+1}{2}(fY' + \phi'F) - 2j(f'Y + F'\phi) - \frac{A_x}{2}(2Y + \eta Y') - \frac{1-j}{2}(f'Y - \phi'F) - LrRe_xYe^{\frac{\theta}{1+\in\theta}} - LrRe_x\phi\left(\frac{X}{1+\in\theta} - \frac{\in\theta X}{(1+\in\theta)^2}\right)e^{\frac{\theta}{1+\in\theta}} = 0, \tag{24}$$

$$f'(\xi,0) = 1,\ g(\xi,0) = 0,\ \theta(\xi,0) = 1,\ \phi(\xi,0) = 1,$$
$$f'(\xi,\infty) = \omega,\ g(\xi,\infty) = 0,\ \theta(\xi,\infty) = 0,\ \phi(\xi,\infty) = 0. \tag{25}$$

$$\begin{aligned} &F'(\xi,0)=0,\ G(\xi,0)=0,\ X(\xi,0)=0,\ Y(\xi,0)=0,\\ &F'(\xi,\infty)=0,\ G(\xi,\infty)=0,\ X(\xi,\infty)=0,\ Y(\xi,\infty)=0. \end{aligned} \tag{26}$$

The physical engineering quantities of interest in this problem are the Skin-friction coefficients in the x- and z-directions, the local Nusselt number (Nu_x) and the Sherwood number (Sh_x) which are given respectively by the following expressions. Taking advantage of the velocity field, the skin friction coefficient at the wall can be obtained in the form

$$Cf_x = -\frac{2\mu\left(\frac{\partial u}{\partial y}\right)_{y=0}}{\rho U_w^2} = -2Re_x^{\frac{-1}{2}} f''(\xi,0), \tag{27}$$

$$Cf_z = \frac{2\mu\left(\frac{\partial w}{\partial y}\right)_{y=0}}{\rho U_w^2} = 2Re_x^{\frac{-1}{2}} g'(\xi,0). \tag{28}$$

Using the temperature field, the rate of heat transfer coefficient can be obtained which in non-dimensional form is given by

$$Nu_x = \frac{xq_w}{\kappa(T_w - T_\infty)} = -Re^{\frac{1}{2}}\theta'(\xi,0), \tag{29}$$

where $\tau_x = \mu\left(\frac{\partial u}{\partial y}\right)_{y=0}$, $\tau_z = \mu\left(\frac{\partial w}{\partial y}\right)_{y=0}$ are the wall shear stresses, $q_w = \kappa\left(\frac{\partial T}{\partial y}\right)_{y=0} + (q_r)_w$ is the wall heat flux as given by Akinbobola and Okoya [37], Bataller [34] and Fatunmbi *et al.* [26], $q_r = -\frac{16\sigma^*}{3K^*}T_\infty^3\frac{\partial T}{\partial y}$. Also with the knowledge of the concentration field, the rate of mass transfer coefficient can be obtained which in non-dimensional form,in terms of Shearwood number is given by

$$Sh = -\phi'(\xi,0)Re_x^{\frac{1}{2}}. \tag{30}$$

3. MATHEMATICAL SOLUTION

The numerical solutions of the dimensionless governing coupled non-linear differential equations (17)-(24) subject to the boundary conditions (25) and (26) derived by the local nonsimilarity approach have been carried out by employing Midpoint Method embedded with Richardson Extrapolation (MMRE) Enhancement scheme implemented, an inbuilt numerical method for boundary value problem on the MAPLE 18 platform which is a symbolic and numeric environment due to its ability to handle highly nonlinear problem of this nature. From this process of numerical computation, the skin-friction coefficients, the Nusselt number and Sherwoood number which correspond to $-f''(\xi,0)$, $g'(\xi,0)$, $-\theta'(\xi,0)$ and $-\phi'(\xi,0)$

respectively are also obtained out and their numerical values are presented in a tabular form.

4. RESULTS AND DISCUSSION

In order to validate the accuracy of our numerical solution by MMRE, comparison is made with the SLLM approximate results and it is clearly seen from the Tables 1 - 5 that an excellent agreement between the results of the two methods are observed.

Table 1 shows a comparative study of present result with MMRE and the SLLM approximate results for some selected values of the unsteadiness parameter A_x. It shows that an increase in the unsteadiness parameter leads to increases in the skin-friction coefficients in both directions. It is clearly seen that the axial and transverse skin-frictions are accurate and precise at 5 decimal places. The negative values of $-f''(\xi, 0)$ mean that the solid surface exerts a drag force on the fluid. This is due to the development of the velocity boundary layer which in the current study is caused solely by the stretching sheet velocity. Moreover, the local Nusselt number (heat transfer coefficient) increases with increase in the unsteadiness parameter. The appreciable increase in Nusselt number shows that heat is being transferred over time with increase in unsteadiness parameter A_x. The calculated slope values of the linear regression (SLR) line through data points for SLLM and MMRE are 0.29224 and 0.20422 slope respectively. It has been observed that many authors have committed the error of neglecting thermal radiation which has been part of the governing equation that should equally be incorporated into the wall heat flux for proper analysis of the Nusselt number according to Bataller [34] and Fatunmbi *et al* [26]. The noticed discrepancies in the heat transfer coefficients may also be due to unperceived error from the previous authors which this research has revealed and addressed. Thus, the MMRE compares favourably with SLLM and the result is in good agreement for skin friction in both directions, which places the MMRE on a good footing than SLLM.

Table 1. Comparison of the Midpoint Method with Richardson Extrapolation Enhancement (MMRE) results of $-f''(\xi,0)$, $g'(\xi,0)$ and $-\theta'(\xi,0)$ with those obtained by Spectral Local Linearization Method (SLLM) when $Pr = 0.72$, $j = m = M = R = \delta = 1$ and $\omega = Lr = Sc = Re_x = Gr_x = Gc_x = \xi = 0$.

	$-f''(\xi,0)$ Shateyi Present [15] Result		$g'(\xi,0)$ Shateyi Present [15] Result		$-\theta'(\xi,0)$ Shateyi Present [15] Result	
A_x	(SLLM)	(MMRE)	(SLLM)	(MMRE)	(SLLM)	(MMRE)
1	2.06334	2.0633409	0.17552	0.1755163	0.95974	0.9488611
2	2.27278	2.2727768	0.15185	0.1518542	1.30759	1.1780898
3	2.46650	2.4664970	0.13459	0.1345976	1.54422	1.3572989

Table 2. Comparison of the Midpoint Method with Richardson Extrapolation Enhancement (MMRE) results of $-f''(\xi,0)$, $g'(\xi,0)$ and $-\theta'(\xi,0)$ with those obtained by Spectral Local Linearization Method (SLLM) when $Pr = 0.72$, $j = m = R = A_x = \delta = 1$ and $\omega = Sc = Re_x = Gr_x = Gc_x = \xi = 0$.

	$-f''(\xi,0)$ Shateyi Present [15] Result		$g'(\xi,0)$ Shateyi Present [15] Result		$-\theta'(\xi,0)$ Shateyi Present [15] Result	
M	(SLLM)	(MMRE)	(SLLM)	(MMRE)	(SLLM)	(MMRE)
1	2.06334	2.0633409	0.17552	0.1755163	0.51730	0.5175441
3	2.40060	2.4005980	0.41758	0.4175784	0.46088	0.4623551
5	2.69188	2.6918781	0.59380	0.5938049	0.43117	0.4275275

In Table 2, we present a comparison between the MMRE and SLLM results for the effect of the magnetic parameter on the skin friction coefficients and the Nusselt number. The implication of the presence of magnetic parameter is that it exert magnetic field on the flow properties and as such as the magnetic strength increases, the skin friction in both directions increase as a result of the dragging effect. Conversely, increase in the value of magnetic parameter lower the Nusselt number. It is observed that increase in the value of magnetic parameter lowers the Nusselt number which in turn increases heat diffusion with the fluid flow as such heat transfer is physically reduced at the wall as M is increased. The calculated slope values of the linear regression (SLR) line through data points for SLLM and MMRE are -0.0215325 and -0.0225042 slope respectively. The implication of this is that application of a strong magnetic field reduces the velocity which in turn increases

heat diffusion with the fluid flow as such heat transfer is physically reduced at the wall as M is increased. MMRE compared favourably with SLLM and the result is in excellent agreement for local skin friction in both directions as their SLR value is thesame for MMRE and SLLM. However, the SLR value of MMRE is lower than that of SLLM.

Table 3. Comparison of the Midpoint Method with Richardson Extrapolation Enhancement (MMRE) results of $-f''(\xi,0)$, $g'(\xi,0)$ and $-\theta'(\xi,0)$ with those obtained by Spectral Local Linearization Method (SLLM) when $Pr = 0.72$, $j = m = R = A_x = \delta = 1.0$ and $\omega = Re_x = Sc = Gr_x = Gc_x = \xi = 0$.

	$-f''(\xi,0)$		$g'(\xi,0)$		$-\theta'(\xi,0)$	
	Shateyi	Present	Shateyi	Present	Shateyi	Present
	[15] Result		[15] Result		[15] Result	
m	(SLLM)	(MMRE)	(SLLM)	(MMRE)	(SLLM)	(MMRE)
0.1	2.2059	2.2059164	0.0312	0.0312785	0.4978	0.4974593
0.5	2.1537	2.1536683	0.1311	0.1311253	0.5041	0.5036479
1.0	2.0633	2.0633410	0.1755	0.1755163	0.5173	0.5162056

In the same vein, Table 3 shows the influence of the Hall current on the skin friction coefficients as well as the Nusselt number. The skin friction coefficient in axial direction is reduced as the values of the Hall current parameter increase. However, the skin friction in transverse direction increases as the Hall current parameter increases. There is slight effect of the Hall current parameter on the Heat transfer rate on the stretching surface only that MMRE values are a bit higher than SLLM.

The variation of $-f''(\xi,0)$, $g'(\xi,0)$, $-\theta'(\xi,0)$ and $-\phi'(\xi,0)$ with respect to chemical reaction parameter Lr, streamwise point ξ, Magnetic strength parameter M, Hall current parameter m, pressure gradient parameter j, Prandtl number Pr and Schmidt number Sc are displayed in Table 4. It is observed from Table 4 that axial skin friction coefficient $-f''(\xi,0)$ increases with increasing chemical reaction parameter, Magnetic strength parameter, Hall current parameter, Prandtl number and Schmidt number meaning that these parameters contributes to the skin friction but decreases with increasing j and ξ. Moreover, the transverse skin friction coefficient $g'(\xi,0)$ increases with increasing values of magnetic strength parameter M, as the magnetic strength increase, the dragging effect is clearly seen by significant increase in the skin friction but reduces with increasing Lr, ξ, m, Pr, Sc and j .

Table 4. Computation showing $-f''(\xi,0)$, $g'(\xi,0)$, $-\theta'(\xi,0)$ and $-\phi'(\xi,0)$ when $R = Re_x = A_x = \delta = 1.0$, $\epsilon = 0.01$, $\omega = 0.02$,$f_w = 0.5$ and $Gr_x = Gc_x = 0.2$.

Pr	Sc	j	m	M	ξ	Lr	$-f''(\xi,0)$	$g'(\xi,0)$	$-\theta'(\xi,0)$	$-\phi'(\xi,0)$
0.72	0.62	1	1	1	2	1	0.14988	0.02459	0.63888	1.77649
0.72	0.62	1	1	1	2	2	0.15774	0.02389	0.63741	2.16347
0.72	0.62	1	1	1	2	3	0.16329	0.02346	0.63645	2.49630
0.72	0.62	1	1	1	1	1	0.22930	0.15851	0.71034	1.84060
0.72	0.62	1	1	1	2	1	0.14988	0.02459	0.63888	1.77649
0.72	0.62	1	1	1	3	1	0.07453	-0.10847	0.57020	1.71319
0.72	0.62	1	1	2	2	1	0.52811	0.34282	0.55461	1.29635
0.72	0.62	1	1	3	2	1	0.84488	0.52729	0.47619	1.24961
0.72	0.62	1	1	4	2	1	1.10659	0.65462	0.40873	1.21150
0.72	0.62	1	2	1	2	1	0.13883	-0.12293	0.69903	1.79844
0.72	0.62	1	3	1	2	1	0.23207	-0.25228	0.71449	1.80534
0.72	0.62	1	4	1	2	1	0.25948	-0.33429	0.71743	1.80711
0.72	0.62	0.5	1	1	2	1	0.59980	0.19091	0.31169	1.65824
0.72	0.62	1.0	1	1	2	1	0.14988	0.02459	0.63888	1.77649
0.72	0.62	1.5	1	1	2	1	-0.41923	-0.38538	0.88631	1.93250
0.72	0.24	1	1	1	2	1	0.12676	0.02721	0.64413	1.08379
0.72	0.50	1	1	1	2	1	0.14482	0.02509	0.63992	1.588923
0.72	0.62	1	1	1	2	1	0.14988	0.02459	0.63888	1.77649
0.24	0.62	1	1	1	2	1	0.09352	0.03206	0.10181	1.85654
0.50	0.62	1	1	1	2	1	0.14988	0.02459	0.63888	1.77649
0.72	0.62	1	1	1	2	1	0.16167	0.02287	0.85198	1.75806

Also, Nusselt number $-\theta'(\xi,0)$ decreases with increasing Lr, ξ, M, Sc and j the interpretation of this is that these parameter reduce heat transfer but increases with increasing Pr, m and j reason been that the Prandtl number, Hall current parameter and pressure gradient parameter contribute to the heat transfer in the system. Furthermore, Shearwood number $-\phi'(\xi,0)$ decreases with increasing ξ, M and Pr, while it increases with Lr, m, Sc and j.

Table 5 shows the behaviour of $-f''(\xi,0)$, $g'(\xi,0)$, $-\theta'(\xi,0)$ and $-\phi'(\xi,0)$ with respect velocity ratio ω, local solutal Grashof number Gc_x, local thermal Grashof number Gr_x, heat source parameter δ, unsteadiness parameter A_x and radiation parameter R. The contribution of local thermal Grashof number Gr_x, local solutal Grashof number Gc_x and heat source parameter δ on $-f''(\xi,0)$ are seen in Table 5 that an increase in Gr_x, Gc_x and δ reduce the axial skin friction, this may be due to thermal and solutal buoyancy force overcoming the skin friction but aid heat and mass transfer as effect is observed on $g'(\xi,0)$, $-\theta'(\xi,0)$ and $-\phi'(\xi,0)$ except only that the heat source parameter inhibits the heat transfer.

Table 5. Computation showing $-f''(\xi,0)$, $g'(\xi,0)$, $-\theta'(\xi,0)$ and $-\phi'(\xi,0)$ when $Pr = 0.72$, $\epsilon = 0.01$, $\omega = 0.02$, $Sc = 0.62$,$f_w = 0.5$, $j = R_x = m = M = 1$ and $Lr = 2$.

R	A_x	δ	Gr_x	Gc_x	ω	$-f''(\xi,0)$	$g'(\xi,0)$	$-\theta'(\xi,0)$	$-\phi'(\xi,0)$
1	1	1	0.2	0.2	0.20	0.17931	0.02374	0.63632	1.34795
1	1	1	0.2	0.2	0.50	0.17963	0.02410	0.63617	1.34788
1	1	1	0.2	0.2	0.70	0.17983	0.02435	0.63607	1.34783
1	1	1	0.2	0.1	0.02	0.17912	0.02353	0.63642	1.34799
1	1	1	0.2	0.5	0.02	0.09918	0.02773	0.64564	1.35588
1	1	1	0.2	1.0	0.02	0.02018	0.03176	0.65447	1.36352
1	1	1	0.1	0.2	0.02	0.19542	0.02143	0.63224	1.34517
1	1	1	0.5	0.2	0.02	0.08346	0.02969	0.64949	1.35853
1	1	1	1.0	0.2	0.02	0.02546	0.03727	0.66519	1.37102
1	1	2	0.2	0.2	0.02	0.14929	0.02428	0.83626	1.34796
1	1	3	0.2	0.2	0.02	0.14620	0.02462	0.78475	1.34896
1	1	4	0.2	0.2	0.02	0.13903	0.02565	0.64108	1.35197
1	0.5	1	0.2	0.2	0.02	-0.22214	0.17474	0.67042	1.36548
1	1.0	1	0.2	0.2	0.02	0.13903	0.02565	0.64108	1.35196
1	1.5	1	0.2	0.2	0.02	0.43662	-0.02874	0.62686	1.82549
2	1	1	0.2	0.2	0.02	0.14685	0.02446	0.75818	1.34901
3	1	1	0.2	0.2	0.02	0.13903	0.02565	0.64108	1.35197
4	1	1	0.2	0.2	0.02	0.13337	0.02659	0.56588	1.35408

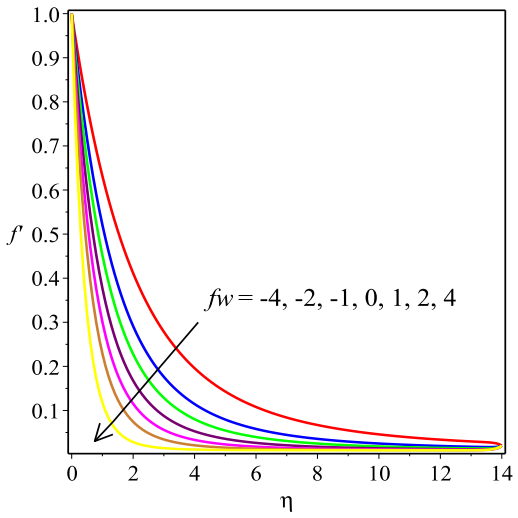

Fig. 2. Axial velocity (f') profiles across the domain at various values of suction (f_w)

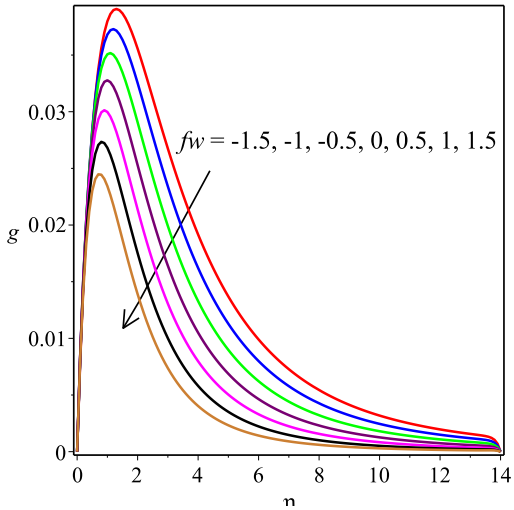

Fig. 3. Transverse velocity (g) profiles across the domain at various values of suction (f_w)

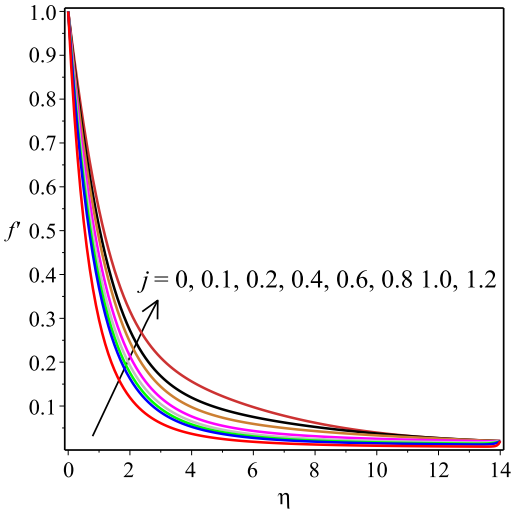

Fig. 4. Axial velocity (f') profiles across the domain at various values of streamwise pressure gradient (j)

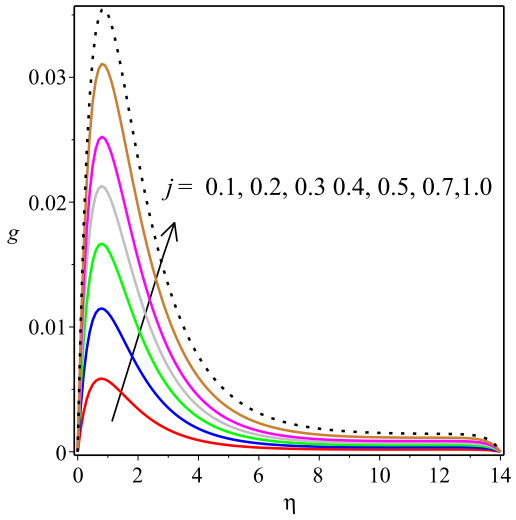

Fig. 5. Transverse velocity (g) profiles across the domain at various values of streamwise pressure gradient (j)

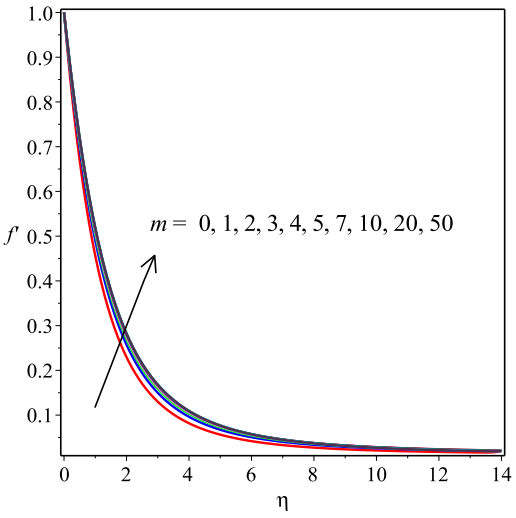

Fig. 6. Axial velocity (f') profiles across the domain at various values of Hall current parameter (m)

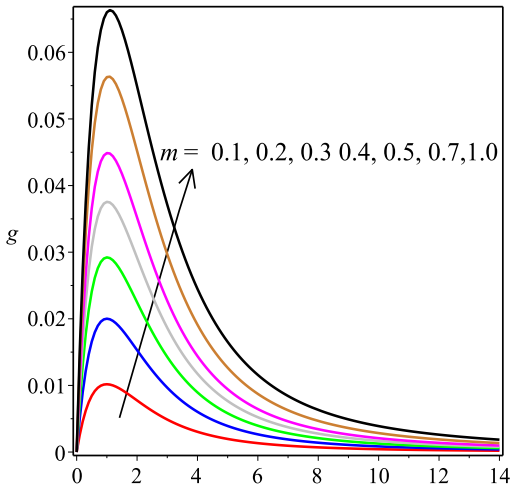

Fig. 7. Transverse velocity (g) profiles across the domain at various values of Hall current parameter (m)

An increase in thermal radiation parameter causes a decrease in axial skin-friction coefficient $-f''(\xi,0)$ and Nusselt number $-\theta'(\xi,0)$ but increase in transverse skin-friction coefficient $g'(\xi,0)$ and Shearwood number $-\phi'(\xi,0)$. Furthermore, the axial skin-friction coefficient $-f''(\xi,0)$ and Shearwood number $-\phi'(\xi,0)$ increase with increase in unsteadiness parameter A_x but results to decrease in $g'(\xi,0)$ and $-\theta'(\xi,0)$. The effect of increase in velocity ratio ω is not that significant on $-f''(\xi,0)$, $g'(\xi,0)$, $-\theta'(\xi,0)$ and $-\phi'(\xi,0)$.

The influence of suction parameter f_w on the axial velocity (f') and transverse velocity (g) are depicted in Figs. 2 and 3 respectively. In both cases, we observe that increasing suction decreases both the axial and transverse velocity profiles. This is physically reasonable since suction, which corresponds to fluid loss (sink) decelerates flow velocity in the flow system. However, the effect of f_w is more felt on the transverse velocity profiles. The observed decrease on both the axial and transverse velocity is due to the nature of dual stretching and suction as was reported by [34]

It is observed in Fig. 4 that the axial velocity profiles increase with increase in the value of j this claim is supported by Dulal *et al* [5]. In Fig. 5, similar behaviour is observed in that the transverse velocity profile increases with increase in j.

Fig. 6 depicts the influence of Hall current parameter m on the axial velocity profiles. However, the Hall current parameter does not have much effects on the except for it large values unlike on

transverse velocity. an attempt to increase m beyond 1.5 (i.e. $m > 1.5$) makes the axial velocity profiles approach the classical values [24]. The effect of the Hall current parameter on the transverse velocity is displayed in Fig. 7, increase in the values of m causes the transverse velocity to rapidly increase owning to the fact that increase in Hall current decreases the viscosity thus increases the velocity of the flow. The presence of Hall current produces Hall effect which contributes to current density and in turn determines magnetic field strength.

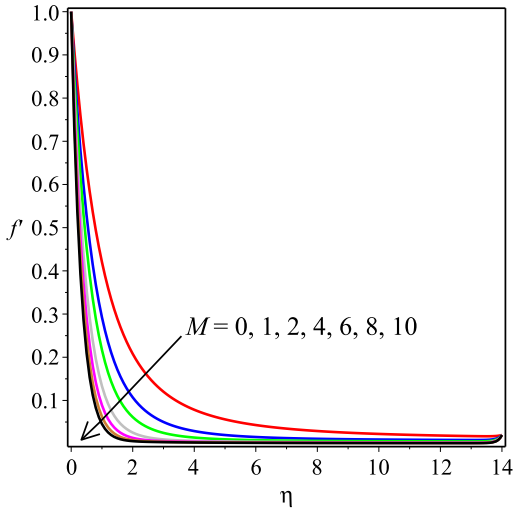

Fig. 8. Axial velocity (f') profiles across the domain at various values of Hartmann number (M)

Fig. 8 depicts the influence of the local Hartmann number M_x on the axial velocity velocity profile, increase in M_x reduces the axial velocity of the fluid. This is because the application of transverse magnetic field will result in a resistive type of force (Lorentz force) similar to drag force which tends to resist the fluid flow and thus reducing its velocity as established by [18], [19] and [28].

Effect of unsteadiness parameter A_x on transverse velocity profiles is shown in Fig. 9. At the initial stage of the flow because of the presence of pressure gradient and buoyancy forces, the transverse velocity profiles are greatly influenced by the unsteadiness (time dependent) parameter A_x in that the flow velocity reduces gradually with time. This observation is physically reasonable and justified.

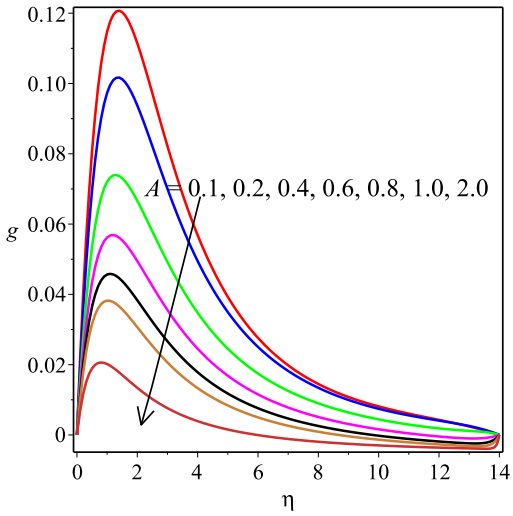

Fig. 9. Transverse velocity (g) profiles across the domain at various values of unsteadiness parameter (A_x)

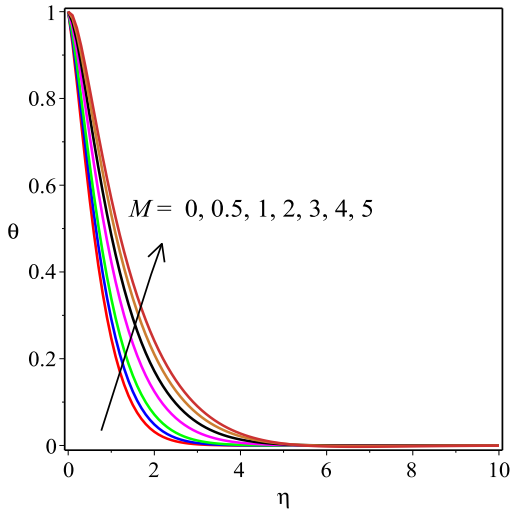

Fig. 10. Dimensionless Temperature (θ) profiles across the domain at various values of Hartmann number (M)

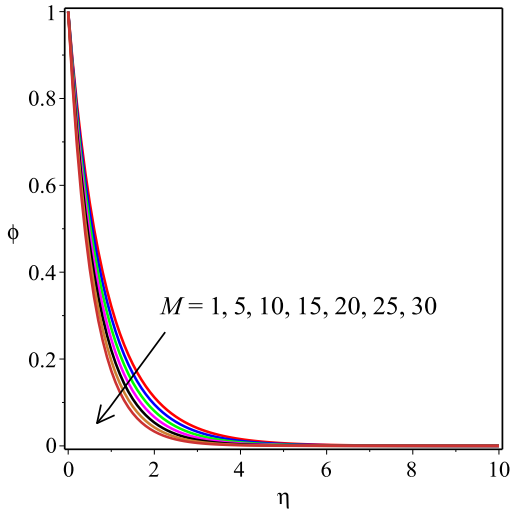

Fig. 11. Dimensionless concentration (ϕ) profiles across the domain at various values of Hartmann number(M)

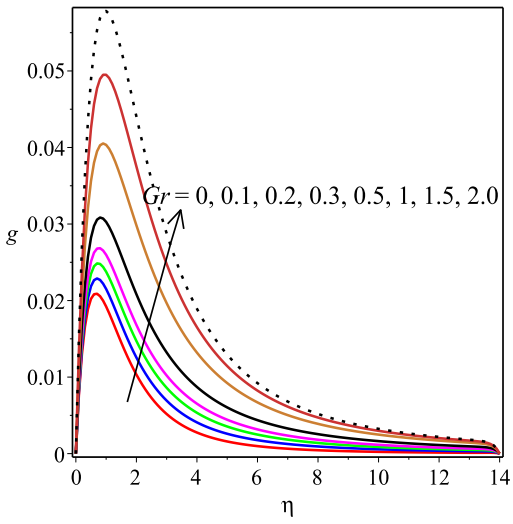

Fig. 12. Transverse velocity (θ) profiles across the domain at various values of thermal Grashof number (Gr)

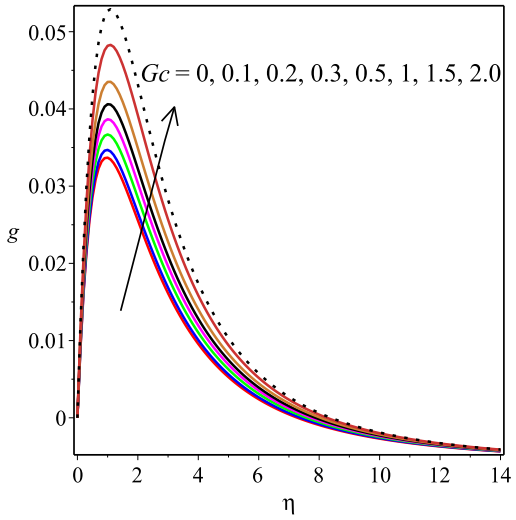

Fig. 13. Transverse velocity (θ) profiles across the domain at various values of solutal Grashof number (Gc)

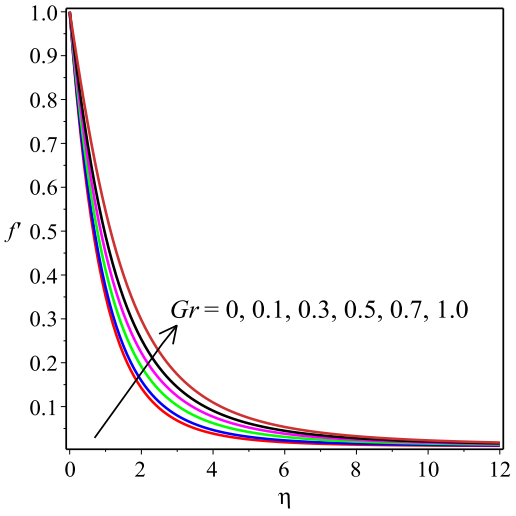

Fig. 14. Axial velocity (f') profiles across the domain at various values of thermal Grashof number (Gr)

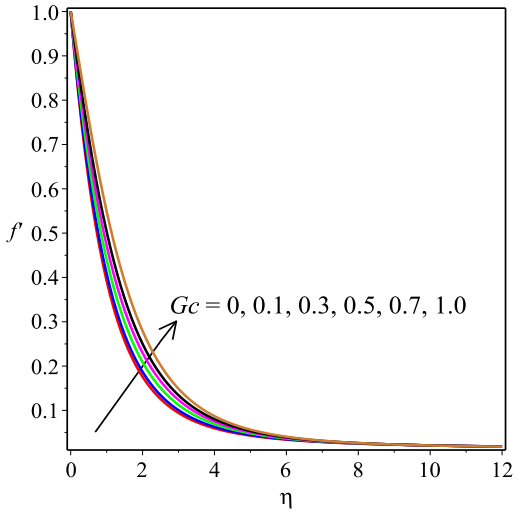

Fig. 15. Axial velocity (f') profiles across the domain at various values of solutal Grashof number (Gc)

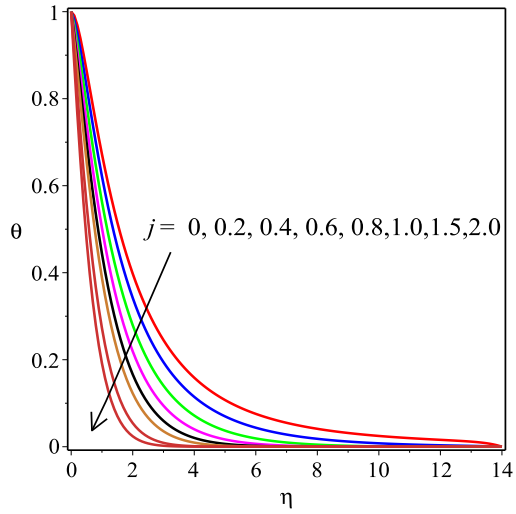

Fig. 16. Dimensionless Temperature (θ) profiles across the domain at various values of pressure gradient parameter (j)

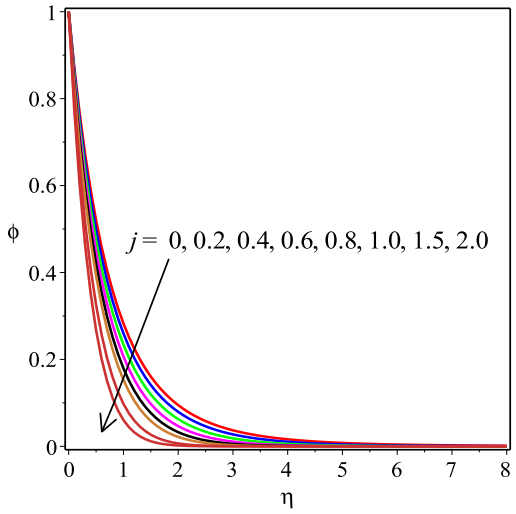

Fig. 17. Dimensionless concentration (ϕ) profiles across the domain at various values of pressure gradient parameter (j)

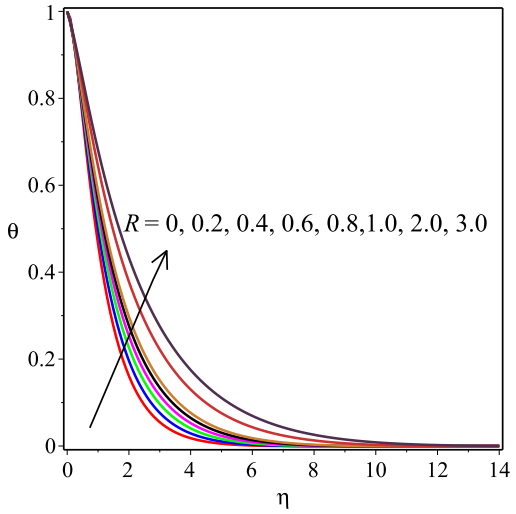

Fig. 18. Dimensionless Temperature (θ) profiles across the domain at various values of thermal radiation parameter (R)

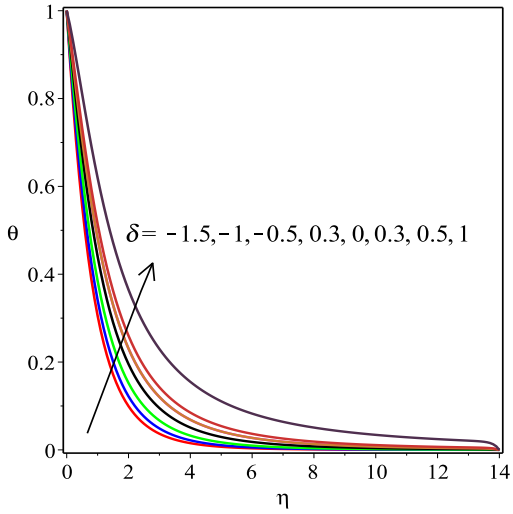

Fig. 19. Dimensionless Temperature (θ) profiles across the domain at various values of heat source parameter (δ)

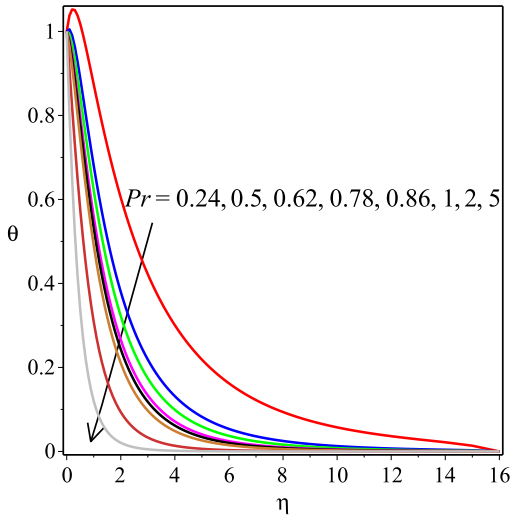

Fig. 20. Dimensionless Temperature (θ) profiles across the domain at various values of Prandtl number (Pr)

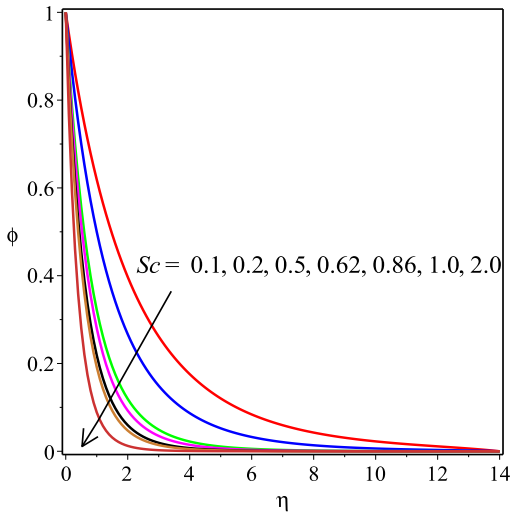

Fig. 21. Dimensionless concentration (ϕ) profiles across the domain at various values of Schmidt number (Sc)

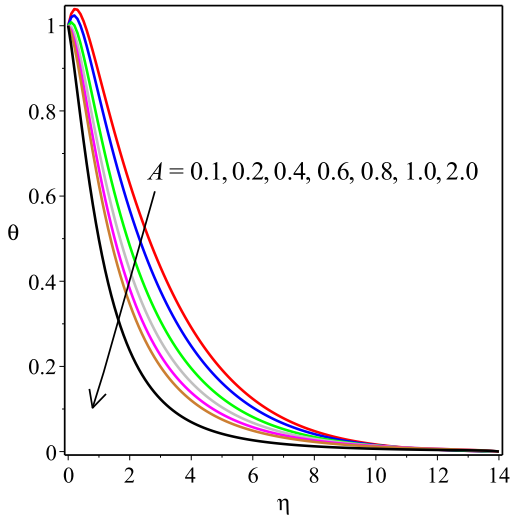

Fig. 22. Dimensionless Temperature (θ) profiles across the domain at various values of unsteadiness parameter (A_x)

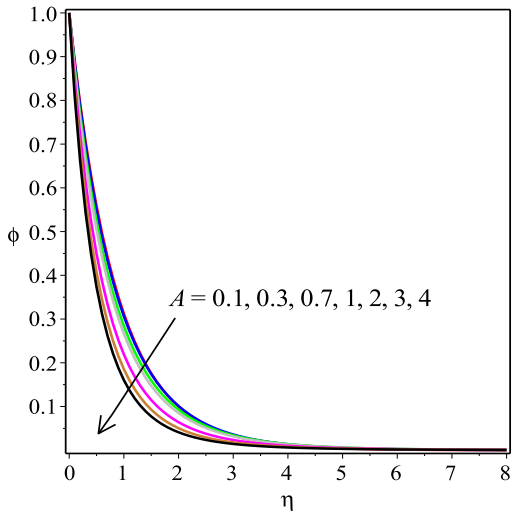

Fig. 23. Dimensionless concentration (ϕ) profiles across the domain at various values of unsteadiness parameter (A_x)

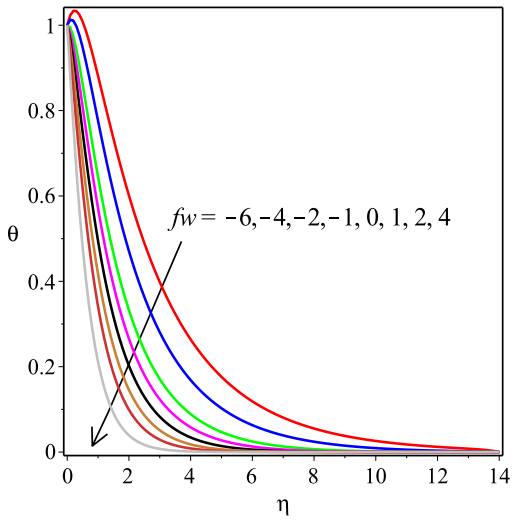

Fig. 24. Dimensionless Temperature (θ) profiles across the domain at various values of suction parameter (f_w)

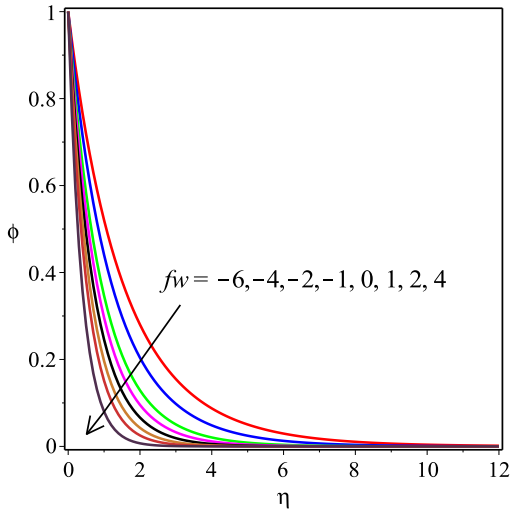

Fig. 25. Dimensionless concentration (ϕ) profiles across the domain at various values of suction parameter (f_w)

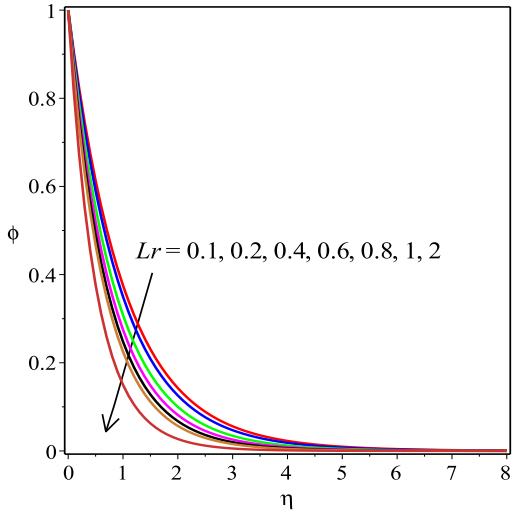

Fig. 26. Dimensionless concentration (ϕ) profiles across the domain at various values of chemical reaction parameter (Lr)

In Fig. 10 the effect of Magnetic strength parameter on the temperature profiles is displayed. The application of a magnetic field to an electrically conducting any fluid produces a kind of drag-like force called Lorentz force. This force causes reduction in the fluid velocity within boundary layer. It is observed that as M increases, the temperature distribution increases. The effect of Lorentz force on velocity profiles generated a kind of friction on the flow (see Fig. 8); this friction in turn generated more heat energy which eventually increases the temperature distribution in the flow.

The effect of magnetic strength parameter M on concentration profiles $\phi(\xi, \eta)$ is displayed in Fig. 11. It is observed that increase in magnetic strength parameter reduces the concentration profiles. This may be due to friction which generating more heat energy that eventually increases the temperature distribution in the flow and therefore the concentration reduces with increase in magnetic strength parameter.

In the Figs. 12 and 13, we observe that the axial velocity profiles increase with increasing buoyancy parameters (Gr_x, Gc_x) leading to an increase in momentum boundary layer thickness. An interesting feature occurs where a velocity spontaneously increase at the reaction source (accelerated flow). In both cases this peak is accentuated with an increase in thermal Grashof number (Gr_x) and solutal Grashof number (Gc_x) at Gr_x or $Gc_x > 0.1$ in the domain $0 < \eta < 3$. Therefore in materials processing systems in order to damp the flow near the moving sheet, lower buoyancy forces are required. The observation in Figs. 12 and 13 is in agreement with the conclusion of a meta-analysis report carried out by Shah [35] on the effects of buoyancy parameters on the flow of different fluids driven by convection over various surfaces. Similar behaviour is seen in Figs. 14 and 15 for the influence of thermal Grashof number and species Grashof number parameter on transverse velocity except that the fluid velocity increase with increasing thermal Grashof number and species Grashof number generally and not concentrated at or near the reaction source or sheet wall.

Fig. 16 shows that the temperature profile increases with increasing j which confirms that the pressure gradient is negative which implies accelerated flow leading to easy convection, hence decrease in temperature. Similarly, Fig. 17 shows the influence of pressure gradient parameter on concentration profile. Fig. 18 depicts the effect of thermal radiation on the temperature profiles. The presence of thermal radiation plays important role on the temperature

such that increase in radiation decreases the temperature profiles [19] and [22]. This observed result may be due to the contribution of heat release/loss of heat energy from the flow system, Therefore, it is noticed that an increase in the thermal radiation parameter results in a decrease in temperature within the boundary layer.

The effect of heat source/sink parameter δ on the temperature profiles is shown in Fig. 19. This result further corroborates what exist in literature and just as expected the heat absorption due to a uniform sink ($\delta < 0$) reduces the temperature and heat generation due to heat source ($\delta > 0$) adds heat and therefore increases temperature of the system which is in agreement with [21] and [24].

In Fig. 20, the effect of Prandtl number Pr on the temperature profiles is shown. The values of Pr are carefully chosen in line with those in literatures varying from small $Pr < 1$ are gases to large $Pr > 1$ which are liquids. It is observed that an increase in Pr reduces the temperature within the boundary layer. This behaviour is as a result of Pr being strongly dependent on thermal diffusivity of fluid from the definition $Pr = \dfrac{\nu}{\alpha}$, meaning that larger Pr has weaker thermal diffusivity which is responsible for a reduction in temperature. The response for species concentration has been computed with an increasing Schmidt number and displayed in Fig. 21, molecular diffusivity will be reduced (low molecular diffusivity) will decrease the ability of the chemical species to diffuse in the regime.

Also the influence of the unsteadiness parameter on the temperature profile is shown in Fig. 22, it is found to have increased with increasing unsteadiness parameter, this observation is in agreement with Ibrahim and Makinde [36] and conversely the concentration profile decreases with increasing unsteadiness parameter as observed in Fig. 23. From Fig. 24 it is seen that the wall suction affects the temperature distribution. Thus, an increase in suction increases temperature which implies that the thermal boundary layer thickness increases. Similarly, in Fig. 25, it is observed that the concentration profile increase with increasing suction. The effect of Chemical reaction parameter L_r on the concentration is seen Fig. 26, it is observed that increase in chemical reaction parameter leads to decrease in concentration profile.

4. CONCLUDING REMARKS

This paper deals with the theoretical study and analysis of heat and mass transfer for a two-dimensional unsteady, chemically reactive MHD mixed convective flow past a stretching sheet in the presence of Hall current. The governing nonlinear partial differential equations have been reduced to a system of coupled nonlinear ordinary differential equations by using a standard nonsimilarity transformation. The resulting equations are then solved numerically using the Midpoint method based on Richardson Extrapolation Enhancement scheme. The results are subjected to analysis using some embedded parameters in the system and displayed graphically. The following conclusions were drawn from the study:

(i) The MMRE compares favourably with SLLM in that an excellent agreement was observed at 5 decimal places.
(ii) The axial and transverse velocities are enhanced when the Hall current parameter increases while the increase in chemical reaction parameter decreases the concentration profile.
(iii) An increase in suction reduces the axial and transverse velocities, temperature and concentration profiles.
(iv) An increase in the thermal and solutal Grashof number increases the axial and transverse velocities; increase in unsteadiness parameter reduces the transverse velocity, temperature and concentration profiles; increase in pressure gradient parameter increases the axial and transverse velocities but reduces the temperature and concentration profiles; increase in thermal radiation and Prandtl number reduces concentration profiles; increase in Schmidt number reduces concentration profiles and high heat source parameter increases the temperature profiles; also an increase in magnetic strength parameter reduces the axial velocity and concentration but increases the temperature profiles.

ACKNOWLEDGEMENTS

The author would like to thank the anonymous referees whose comments improved the original version of this manuscript.

NOMENCLATURE

a, b, c	initial stretching rate, stretching rate, positive constant respectively
A_x	ratio of stretching rate or unsteadiness parameter
B_o	applied uniform transverse magnetic field strength
C	dimensional species concentration of the fluid
C_w	species concentration of the fluid along the sheet wall
C_∞	species concentration of the fluid far away from the sheet wall
C_p	specific heat capacity at constant pressure
D	effective diffusive coefficient or mass diffusion coefficient
E	activation energy
f	dimensionless or reduced stream function,
f'	dimensionless axial velocity variable,
F	auxiliary axial or horizontal velocity function, $\frac{\partial f}{\partial \xi}$,
g	dimensionless transverse or vertical velocity function,
g^*	acceleration due to gravity
G	auxiliary transverse velocity function, $\frac{\partial g}{\partial \xi}$,
Gr_x	local thermal Grashof number
Gc_x	local Solutal Grashof number
K_T	thermal diffusion ratio
Lr	chemical reaction parameter
m	Hall current parameter
M	Magnetic strength parameter/Local Hartmann number
P	pressure
Pr	Prandtl number
R	thermal radiation parameter
R^*	universal gas constant
Re_x	local Reynolds number
Sc	Schmidt number
t	time
T	dimensional temperature of the fluid
T_m	mean fluid temperature
T_w	temperature of the sheet wall
T_∞	dimensional or free stream temperature of the fluid far away from the sheet
u, v, w	velocity components in x, y and z direction respectively
U_w	velocity at the sheet wall or mainstream velocity
U_∞	velocity far away from the sheet wall or free stream velocity
X	auxiliary dimensionless temperature function, $\frac{\partial \theta}{\partial \xi}$,
Y	auxiliary dimensionless concentration function, $\frac{\partial \phi}{\partial \xi}$,

Greek Symbols

ρ fluid density
σ electrical conductivity of fluid
α thermal diffusivity
μ dynamic viscosity
ν kinematic fluid viscosity
κ constant thermal conductivity
δ heat source/sink parameter
θ dimensionless temperature
ϕ dimensionless concentration
β_T thermal expansion(volumentric) coefficient
β_c concentration expansion coefficient
η pseudo-similarity variable
ξ non-similarity variable

Subscripts and Superscripts

w condition at the wall
j exponent of nonlinear stretching velocity/streamwise pressure gradient parameter.

REFERENCES

[1] B. C. Sakiadis, *Boundary-layer equations for two-dimensional and axisymmetric flow*, Boundary-layer Behaviour on Continuous Solid Surface I, AICHE J, **7**, 26-28, 1961.

[2] B. C. Sakiadis, *Boundary-layer behaviour on continuous flat surface*, Boundary-layer Behaviour on Continuous Solid Surface II, AICHE J, **7**, 221-225, 1961.

[3] J. A. Dantzig and C. L. Tucker, *Modeling in in Materials Processing*, Cambridge University Press. 1900.

[4] A. S. P. Devi and R. Kandasamy, *Effects of heat and mass transfer on MHD laminar boundary layer flow over a wedge with suction or injection*, Journal of Energy Heat and Mass Transfer, **2**, 167, 2001.

[5] P. Dulal and M. Hiranmoy, *Influence of temperature-dependent viscosity and thermal radiation on MHD forced convection over a no-isothermal wedge*, Applied Mathematics and Combustion, **212**, 194-–208, 2009.

[6] T. Fang and J. Zhang, *Flow between two stretchable disks - an exact solution of the Navier-Stokes equation*, International Communication in Heat and Mass Transfer, **35**, 892-–895, 2008.

[7] A. D. Fitt and C. P. Please, *Asymptotic analysis of the flow of shear-thinning foodstuffs in annular scraped heat heat exchangers*, J. Engineering Mathematics, **39**, 345-366, 1900.

[8] T. Haga and S. Suzuki, *A downward melt drag single roll caster for casting semisolid slurry*, J. Materials Processing Technology, **157**, 695-700, 2004.

[9] B. G. Hildebrand, S. G. Sterling and M. A. Price, *An evaluation of three material models used in the finite element simulation of a sheet stretching process*, J Materials Processing Technology, **103**, 57-64, 2000.

[10] C. Y. Wang, *Liquid film on an unsteady stretching sheet*, Quarterly of Applied Mathematics, **48**(4), 601-–610, 1990.

[11] P. K. Kundu, I. M. Cohen and D. R. Dowling, *Fluid Mechanics*. Fifth edition, Elsevier, The Boulevard, Langford Lane Kidlington, Oxford, UK, 369-–375, 2012.

[12] T. Watanabe and I. Pop, *Thermal boundary layers in magnetohydrodynamics flow over a flat plate in the presence of a transverse magnetic field*, Acta Mech, **105**, 233-–238, 1994.

[13] N. G. Kafoussias and N. D. Nanousis, *Magnetohydrodynamic laminar boundary layer flow over a wedge with suction or injection*, Can. J. Phys., **75**, 787-–792, 1997.

[14] E. H. Hall, *On a new action of the magnet on electric currents*, American Journal of Mathematics, **2**(3), pages 287 – 292, 1879.

[15] G. W. Sutton and A. Sherman, *Engineering Magnetohydrodynamics*, McGraw-Hill, New York, 1965.

[16] H. Alfven, *Existence of electromagnetic-hydromagnetic waves*, Nature Publishing Group, **150**(3805), 405 - 406, 1942.

[17] V. J. Rossow, *On Flow of electrically conducting fluid over a flat plate in the presence of a transverse magnetic field*, National Advisory Committee for Aeronautics Technical Report, **1358**, 489-508, 1957.

[18] R. Muthucumaraswamy, *Effect of a chemical reaction on a moving isothermal vertical surface with suction*, Acta Ciencia Indica, **155**, 65—70, 2002.

[19] R. L. V. R. Devi, T. Poornima, N. B. Reddy and S. Venkataramana, *Radiation and mass transfer effects on MHD boundary layer flow due to an exponentially stretching sheet with heat source*, IJEIT, **3**(8), 33—38, 2014.

[20] K. Gangadhar and R. N. Bhaskar, *Chemically reacting MHD boundary layer flow of heat and mass transfer over a moving vertical plate in a porous medium with suction*, Journal of Applied Fluid Mechanics, **6**(1), 107—114, 2013.

[21] K. Bhattacharyya *Effects of heat source/sink on MHD flow and heat transfer over a shrinking sheet with mass suction*, Chemical Engineering Research Bulletin, **15**, 12—17, 2011.

[22] T. S. Reddy, O. S. P. Reddy, M. C. Raju and S. V. K. Varma *MHD free convection heat and mass transfer flow through a porous medium bounded by a vertical surface in presence of Hall current*, Advances in Applied Science Research, **3**(6), 3482-3490, 2012.

[23] O. D. Makinde, K. Zimba and O. A. Beg *Numerical Study of Chemically-Reacting Hydromagnetic Boundary Layer Flow with Soret/Dufour Effects and a Convective Surface Boundary Condition*, Int. J. of Thermal and Environmental Engineering, **4**(1), 89-98, 2012.

[24] S. Shateyi and M. Gerald, *Hall Effect on MHD flow and heat transfer over an unsteady stretching permeable surface in the presence of thermal radiation and heat Source/Sink*, Journal of Applied Mathematics, **2008**, 1-12, 2014.

[25] B. M. Rao , G. V. Reddy, M.C. Raju, S.V.K. Varma, *MHD Transient free convection and chemically reactive flow past a porous vertical plate with radiation and temperature gradient dependent heat source in slip flow regime*, IOSR Journal of Applied Physics (IOSR-JAP), **3**(6), 22-32, 2013.

[26] E. O. Fatunmbi, S. S. Okoya and O. D. Makinde, *Convective heat transfer analysis of hydromagnetic micropolar fluid flow past an inclined nonlinear stretching sheet with variable thermophysical properties*, Diffusion Foundations, ISSN: 2296-3642, **26**, 63-77, 2020.

[27] A. Ishak, R. and I. Pop, *Heat transfer over an unsteady stretching permeable surface with prescribe wall temperature*, Nonlinear Analysis: Real World applications, **10**, 2909-2913, 2009.

[28] S. Khan, I. Karim and H. A. Biswas, *Heat generation, thermal radiation and chemical reaction effects on MHD mixed convection flow over an unsteady stretching permeable surface*, International Journal of Basic and Applied Science, **1**(2), 350 - 364, 2012.

[29] W. J. Minkowycz and E. M. Sparrow, *Numerical solution scheme for local non-similarity boundary layer analysis*, Numerical Heat Transfer, 1, 69 - 85, 1978.
[30] E. M. Sparrow, H. Quack and C. J. Boerner, *Local non-similarity boundary layer solutions*, American Institute of Aeronautics and Astronatics Journal, **8**(11), 1936-1942, 1970.
[31] E. M. Sparrow and H. S. Yu, *Local non-similarity thermal boundary layer solutions*, Journal of Heat Transfer, **93**, 328-334, 1971.
[32] R. Mohamad, R. Kandasamy and M. Ismoen, *Local non-similarity solution for MHD mixed convection flow of a nanofluid past a permeable vertical plate in the presence of thermal radiation effects*, Journal of Applied and Computational Mathematics, **4**(6), 1-9, 2015.
[33] R. C. Bataller, *Effects of heat source/sink, radiation and work done by deformation on flow and heat transfer of a viscoelastic fluid over a stretching sheet.* Comput Math Appl **53**, 305-316, 2007.
[34] N. A. Shah, I. L. Animasaun, A. Wakif, O. K. Koriko, R. Sivaraj, K. S. Adegbie, Z. Abdelmalek, H. Vaidyaaa, A. F. Ijirimoye and K. V. Prasad, *Significance of suction and dual stretching on the dynamics of various hybrid nanofluids: Comparative analysis between type I and type II models*, Physica Scripta, **95**(9), 1—14, 2020.
[35] N. A. Shah, I. L. Animasaun, R. O. Ibraheem, H. A. Babatunde, N. Sandeep and I. Pop, *Scrutinization of the effects of Grashof number on the flow of different fluids driven by convection over various surfaces*, . Journal of Molecular Liquids, **249**, 980—990, 2017.
[36] W. Ibrahim and O. D. Makinde, *Magnetohydrodynamic stagnation point flow and heat transfer of casson nanofluid past a stretching sheet with slip and convective boundary condition*, Journal of Aerospace Engineering, **29**2, 04015037-1-11, 2016.
[37] T. E. Akinbobola and S. S. Okoya, *The flow of second grade fluid over a stretching sheet with variable thermal conductivity and viscosity in the presence of heat source/sink*, Journal of the Nigerian Mathematical Society, **34**, 331-342, 2015.

DEPARTMENT OF MATHEMATICS, ADEYEMI COLLEGE OF EDUCATION, ONDO, NIGERIA
E-mail address: femathlaw@yahoo.com

DEPARTMENT OF MATHEMATICS, OBAFEMI AWOLOWO UNIVERSITY, ILE - IFE, NIGERIA
E-mail addresses: soajadi@yahoo.co.uk, sajadi@yahoo.com